Final Draft
of the original manuscript:

Zhang, Z.; Rahman, M.; Abetz, C.; Bajer, B.; Wang, J.; Abetz, V.:
Quaternization of a Polystyrene-block-poly(4-vinylpyridine) Isoporous Membrane: An Approach to Tune the Pore Size and the Charge Density.
In: Macromolecular Rapid Communications. Vol. 40 (2019) 3, 1800729.
First published online by Wiley: 12.11.2018

https://dx.doi.org/10.1002/marc.201800729

Quaternization of a Polystyrene-*block*-poly(4-vinylpyridine) Isoporous Membrane: An Approach to Tune the Pore Size and the Charge Density[a]

Zhenzhen Zhang, Md. Mushfequr Rahman, Clarissa Abetz, Barbara Bajer, Jiali Wang, Volker Abetz*

Z. Zhang, Dr. Md. M. Rahman, C. Abetz, B. Bajer, J. Wang, Prof. V. Abetz
Helmholtz-Zentrum Geesthacht
Institute of Polymer Research
Max-Planck-Str. 1, 21502 Geesthacht, Germany
E-mail: volker.abetz@hzg.de
Prof. V. Abetz
University of Hamburg
Institute of Physical Chemistry
Martin-Luther-King-Platz 6, 20146 Hamburg, Germany

Abstract: Isoporous integral asymmetric membranes derived from the self-assembly of block copolymers combined with the non-solvent induced phase separation (SNIPS) have gained great attention. To extend their utility, a good control over pore size and surface functionality in a facile manner is highly desirable. Here an approach is proposed to achieve this by quaternization of the poly(4-vinylpyridine) (P4VP) moiety of a polystyrene-*block*-poly(4-vinylpyridine) (PS-*b*-P4VP) SNIPS membrane using alkyl iodides via a scalable gas-solid heterogeneous reaction. By changing the size of the alkyl groups of the quaternization agent and the degree of quaternization the effective pore size of the membrane is tailored in a wide range from the ultrafiltration to the nanofiltration regime. A quaternization of approx. half of the 4VP repeating units of the membranes with methyl iodide, ethyl iodide, or 1-propyl iodide leads to a retention of methylene blue from a 10 mg L^{-1} aqueous solution of 96%, 87% and 83%, respectively.

FIGURE FOR ToC_ABSTRACT

[a] **Supporting Information** ((bold)) is available online from the Wiley Online Library or from the author.

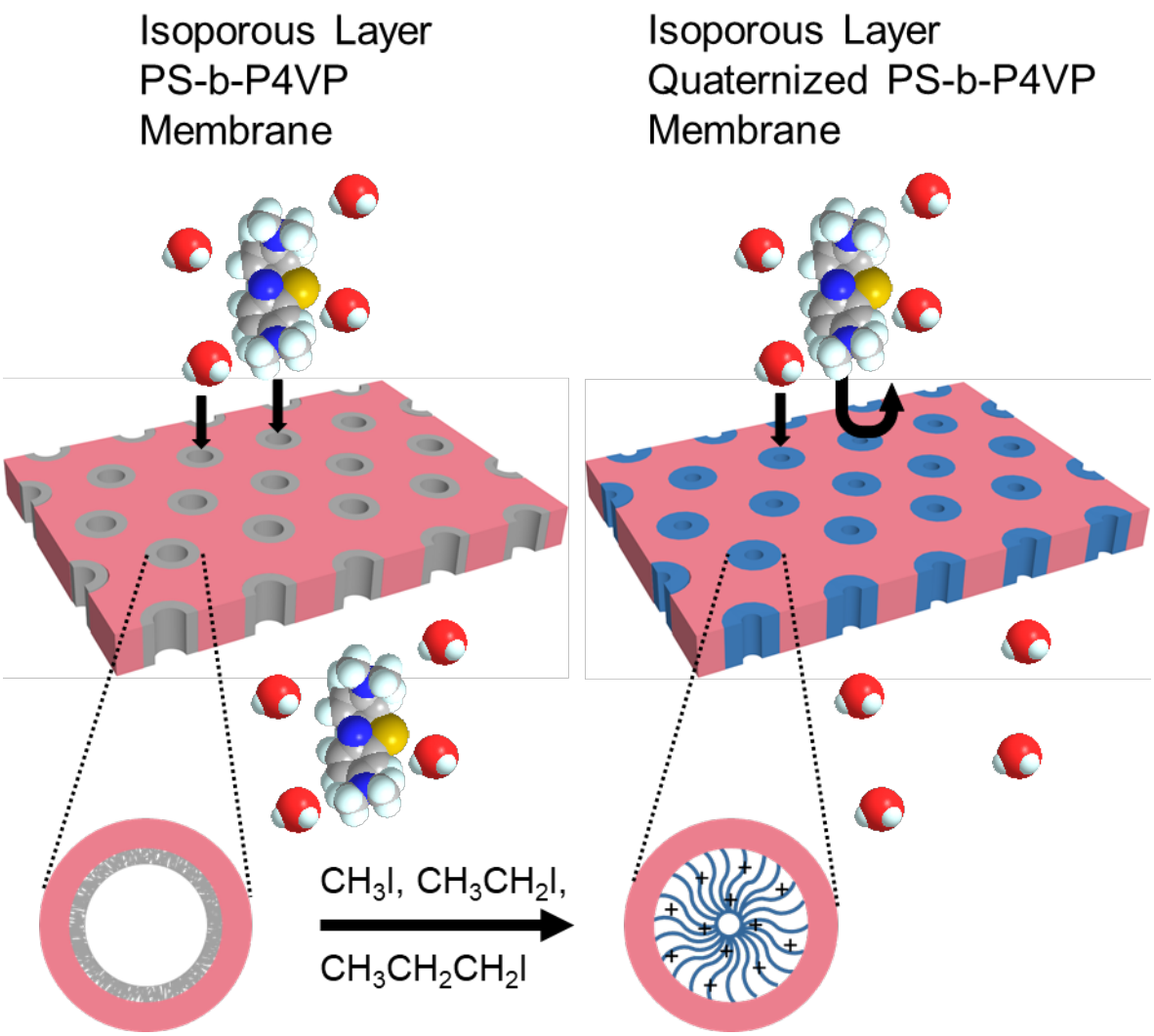
Isoporous Layer
PS-b-P4VP
Membrane
Isoporous Layer
Quaternized PS-b-P4VP
Membrane
CH3I, CH3CH2I,
CH3CH2CH2I

Mesoporous membranes play a significant role in many separations such as biomolecule separation, potable water purification, or wastewater treatment.[1] In these settings, most membranes separate molecules or particles mainly on the basis of size-selectivity. In order to enhance the separation performance, it is crucial to adjust the pore size, and to further understand and control the transport of analytes at the nanoscale. Block copolymers (BCPs) have received great interest for the preparation of advanced membranes with a well-defined mesoscopic structure and high accessible porosity, owing to their ability to self-assemble into a variety of periodic, ordered mesoscale structures.[2] In 2007, a fast one-step scalable technique based on a combination of self-assembly of a block copolymer and non-solvent-induced phase separation (SNIPS) was developed to fabricate BCP derived membranes.[3] Resulting membranes typically have a rather thin (< 200 nm) selective layer with a high density of ordered vertically-aligned cylindrical pores with narrow pore size distribution on top of a relatively thick spongy substructure comprised of the same material.[4] This integral asymmetric isoporous structure ensures good selectivity while maintaining high permeability. Therefore, over the past decade, the SNIPS technique has been applied to a variety of block copolymers in flat sheet geometry.[5] Also efforts were undertaken to reduce the amount of block copolymer when preparing SNIPS membranes in both flat sheet[6] and hollow fiber geometry[7] . Although the SNIPS process is qualitatively understood to a certain extent,[8] it is still not possible to quantitatively predict the pore size and overall integral asymmetric structure of a membrane due to many parameters influencing the structure formation process. However, a few relationships have been found to tailor the pore size of SNIPS membranes. One rather straightforward approach is to vary either the molecular weight or the composition of BCPs.[9] Binary blending of polystyrene-*block*-poly(4-vinylpyridine) (PS-*b*-P4VP) with different molecular weights and compositions has also shown to tailor the pore size according to the different ratio of the blend partners.[10] Another strategy is to begin with a given porous membrane and alter its pore properties or pore size by post treatments, which do not destroy the

basic membrane structure. Yu *et al.* controlled the pore size by electroless gold deposition on PS-*b*-P4VP SNIPS membranes based on physical coordination interaction.[11] Also molecular vapor deposition of aluminum oxide can be used to control the pore size of PS-*b*-P4VP SNIPS membranes.[4] Filling porous block copolymers with inorganic components was also done to introduce for example catalytic functionality[12] or contrast for 3D imaging of the porous block copolymer structure.[13] Post treatment of a PS-*b*-P4VP SNIPS membrane with dopamine and poly(*N*-isopropyl acrylamide) led to a temperature and pH-repsonsive membrane.[14] Based on a dopamine functionalization also atom transfer radical polymerization (ATRP) of poly(2-hydroxylethyl methacrylate) (PHEMA) was carried out on a PS-*b*-P4VP SNIPS membrane.[15] Physical and chemical routes of post treatment were also introduced to reduce the pore size of a PS-*b*-PHEMA SNIPS membrane by thermal treatment or reaction of the hydroxyl groups with an alkyl isocyanate, respectively.[16]

In recent years efforts have been made to reduce the pore size in the nanofiltration regime by taking advantage of the swelling of the pore-forming block in the hydrated state. As P4VP and P2VP are pH responsive, the nitrogen moieties are protonated at low pH which leads to stretching of the P4VP and P2VP block in corresponding block copolymers.[5a, 14, 17] Gu *et al*. demonstrated that the pore size of a polyisoprene-*block*-polystyrene-*block*-poly(4-vinylpyridine) (PI-*b*-PS-*b*-P4VP) membrane can be reduced to 5 nm using an additive driven pore expansion together with chain stretching of the P4VP block at pH 3.6. At neutral pH the pore size of the membrane was around 29 nm, as the P4VP block was in a collapsed state due to deprotonation of the nitrogen moieties.[18] Similarly, Mulvenna *et al*. reported the pore size of a polyisoprene-*block*-polystyrene-*block*-poly(acrylic acid) (PI-*b*-PS-*b*-PAA) membrane can be reduced to 3.4 nm at pH 5.5.[5g] Later, Zhang *et al*. attached sulfonic acid moieties to the pore wall of a PI-*b*-PS-*b*-PAA membrane using carbodiimide coupling. The resulting polyisoprene-*block*-polystyrene-*block*-poly(2-acrylamido-ethane-1,1-disulfonic acid) (PI-*b*-

PS-*b*-PADSA) membrane exhibited a smaller effective pore diameter and lower degree of ionic strength response compared to the PI-*b*-PS-*b*-PAA counterpart.[19] In these works, the tailoring of the pore size is dependent on protonation[18] or deprotonation[5g, 19] of the functional groups of the pore-forming block. PS-*b*-P4VP is a popular membrane material for quaternization due to the lone pair electron of the nitrogen of P4VP block.[20] Unlike a protonated P4VP block, swelling of the quaternized P4VP block in the hydrated state is not limited to acidic conditions. Quaternized PS-*b*-P4VP membranes showing good anti-fouling properties[21] and selective separation of proteins[22] were reported. Herein, we present for the first time a versatile strategy for constructing an adjustable pore size and surface functionality of a PS-*b*-P4VP SNIPS membrane via a facile quaternization reaction using alkyl iodides with different sizes of alkyl groups (i.e. methyl iodide (MeI), ethyl iodide (EtI) and 1-propyl iodide (1-PrI)) (Figure 1a).

To retain the original integral asymmetric isoporous structure, the quaternization has to be employed under a mild heterogeneous condition, for instance, by using a non-solvent as the reaction medium[22] or a vapor-phase reaction without any solvent.[21, 23] In this study, a facile and scalable gas-solid interface reaction was selected to carry out the quaternization of a PS-*b*-P4VP membrane. The degree of quaternization with MeI, EtI and 1-PrI was controlled quantitatively by varying the duration of reaction (Supporting Information, Figure S3 – Figure S5) and the morphology of the quaternized membranes was monitored by scanning electron microscopy (SEM) (Supporting Information, Figure S6 – S10). The FTIR spectra, ^{1}H NMR spectra and SEM micrographs of the pristine PS-*b*-P4VP membrane (I0) and the 100% quaternized PS-*b*-P4VP membrane with MeI (M100) are depicted in **Figure 1**. In the FTIR spectrum (Figrue 1b), I0 showed a characteristic peak at ca. 1600 cm^{-1} due to the stretching vibration of C=N and C=C of the aromatic rings. M100 showed a characteristic peak for the C=N^{+} stretching vibration at ca. 1640 cm^{-1}.[24] Since after quaternization the stretching vibration of C=N had disappeared, the intensity of stretching vibration at ca. 1600 cm^{-1} became

much weaker than in the spectrum of I0. Moreover, a broad signal appeared at ca. 3400 cm^{-1} due to water molecules associated with the quaternized 4VP groups. In the ^{1}H NMR spectrum of I0 the chemical shift at 8.75 ppm (peak a) was ascribed to two protons of unquaternized pyridine groups. The characteristic chemical shifts at 8.95 ppm (peak a′) appeared from two corresponding protons of quaternized pyridine groups in the ^{1}H NMR spectrum of M100 (Figure 1c). M100 clearly retained the integral asymmetric isoporous structure after quaternization (Figure 1d, g). Owing to the extra attachment of alkyl iodide molecules along the pore walls the pores on the top surface of M100 became 22 nm (Figure 1h) while that of I0 was 27 nm (Figure 1e). The back scattered electron (BSE) imaging mode of SEM was used to determine the distribution of the electron rich iodide counterion. The BSE image of the top surface of I0 (Figure 1f) did not show any contrast between the matrix-forming block PS and the pore-forming block P4VP as the atomic number of C and N are next to each other. Whereas, there were brighter rings with uniform thickness along the pore walls of M100, assigned to the electron rich iodide, indicating the homogeneity of quaternization on the top surface (Figure 1i). The cross-sectional image (Supporting Information, Figure S6) also displayed the uniform distribution of iodide, which confirmed the uniform quaternization of the P4VP block all over the membrane.

We have compared the membranes with ca. 52% quaternization of 4VP repeating units by MeI (M52), EtI (E52) and 1-PrI (P52) to investigate the influence of the size of alkyl groups on the morphology and separation performance of the membranes (**Figure 2**). The dynamic contact angle of a water droplet was monitored at the surface of I0, M52, E52, and P52. Figure 2a shows the snapshots of a sinking water droplet at the surface of I0. The snapshots of the water droplets at the surface of M52, E52 and P52 are provided in the Supporting Information Figure S11. In case of I0, the water droplet totally sunk into the membrane after ca. 12 s due to the big open pores. To compare the sinking rate of a water droplet, the contact angle vs time is provided in

Figure 2b. The sinking rate of a water droplet was lower in the quaternized membranes compared to I0, which followed the sequence, M52 < E52 < P52 < I0. The difference in change of contact angle of a water droplet at the surface of these porous membranes (Figure 1a, 1b and S11) implies that these membranes have different resistance against the permeation of a water droplet. To provide further evidence of this phenomenon, the water flux (J_w) through I0, M52, E52 and P52 was determined using a dead-end mode filtration device at a trans-membrane pressure of 1 bar. In accordance with the sinking rate of the water droplet, the water fluxes followed the sequence $J_{wM52} < J_{wE52} < J_{wP52} << J_{wI0}$ (Figure 2c). The average pore size of the isoporous layer of M52, E52 and P52 was 22 – 23 nm (Figure 2 d-f) while that of I0 was 27 nm (Figure 1e) according to SEM images. In spite of such small difference, for the first 2 hours of water flux measurement, J_{wM52} was ca. 52 times lower than J_{wI0} while J_{wP52} was ca. 15 times lower than J_{wI0}. During SEM investigation the pore-forming blocks of the membranes were in a collapsed state as the membranes were completely dry. Owing to their polyelectrolyte nature, the quaternized P4VP blocks of M52, E52 and P52 were dissociated in water, making the pore-forming P4VP block partially charged and significantly swelled during the water flux measurement. As the hydrophobic PS matrix was fixed in space, the repulsive electrostatic interaction among the charged 4VP repeating units induced chain stretching toward the center of the pore, resulting in the smaller effective pore size. The constrained pore size imposed resistance to water penetration through the membrane. Moreover, the water flux through P52 was three times higher compared to that through M52, which proves that the stretching of a P4VP block quaternized by 1-PrI is significantly lower than that quaternized by MeI (Figure 2g). The hydrophilicity of the quaternized P4VP decreases with increasing the size of the alkyl group of the quaternization agent.[25] The lower hydrophilicity of the pore-forming block of P52 leads to lower stretching in a hydrated state compared to that of E52 and M52. Consequently, the effective pore size, the rate of sinking of the water droplet (Figure 2b), and the water flux (Figure 2c) are higher in the case of P52 compared to E52 and M52. The water

flux measurements were carried out for 24 h. A gradual decrease of water flux as a function of time was observed. The average water flux during the first 2 h measurement ((J_{wM52} (13 L m^{-2} h^{-1}) < J_{wE52} (17 L m^{-2} h^{-1}) < J_{wP52} (43 L m^{-2} h^{-1}) << J_{wI0} (675 L m^{-2} h^{-1}))) and during the last 2 h measurement ((J_{wM52} (11 L m^{-2} h^{-1}) < J_{wE52} (13 L m^{-2} h^{-1}) < J_{wP52} (23 L m^{-2} h^{-1}) << J_{wI0} (375 L m^{-2} h^{-1})) showed a similar trend, which proved the quaternization was stable during the water flux measurement (Figure 2c). In previous studies, it was reported that the hydrophilicity of cross-linked membranes containing amine[26] and 4VP[25] moieties can be tuned by changing the size of the alkyl group (methyl, ethyl and 1-propyl) of the quaternization agent. Since in a PS-*b*-P4VP SNIPS membrane only one end of the pore-forming block (P4VP) is attached to the matrix-forming block (PS), we utilized this phenomenon to tailor the effective pore size of the membrane in the hydrated state.

The performance of the membranes was tested by investigation of their separation properties of the cationic dye methylene blue (MB) (MB structure depicted in **Figure 3a**) from aqueous solutions in a dead-end filtration mode. Figure 3b shows that the color of the permeate solution through I0 was similar like the feed solution. In the permeate solutions through M52, E52 and P52 a substantial reduction of color was observed. The concentration of MB in the feed solution C_f (mg L^{-1}) and permeate solutions C_p (mg L^{-1}) was determined via UV-vis spectroscopy (Figure 3c). Figure 3d shows for a 10 mg L^{-1} feed solution that the retentions follow the sequence R_{M52} (96%) > R_{E52} (87%) > R_{P52} (83%) ≫ R_{I0} (~0). Similar to the permeation of water, P52 had the lowest resistance against permeation of MB while M52 had the highest resistance. In general, the rejection of a charged solute originates from a combined effect of size exclusion and electrostatic repulsion with a charged porous membrane.[27] As the retention gradually decreased with increasing effective pore size, it is clear that the retention of MB in M52, E52 and P52 was largely dictated by size exclusion. Figure 3b displays after the dye retention measurement that I0 became bluish in color, indicating the affinity of the cationic dye MB with

the 4VP groups of the membrane. The color changes of M52, E52 and P52 were significantly lower compared to that of I0. Hence, we assume that the quaternized 4VP groups repelled the cationic MB, which also contributed to the high retention of MB. The color difference between I0 and the quaternized membranes M52, E52 and P52 were more obvious when the 100 mg L^{-1} aqueous solution of MB was used for the retention measurement (Supporting Information, Figure S13a). For 100 mg L^{-1} feed solution the values of MB retention were R_{M52} (97%) ≈ R_{E52} (95%) ≈ R_{P52} (96%) >> R_{I0} (6%) which were higher than those for 10 mg L^{-1} feed solution (Supporting Information, Figure S13c). It is well known that the ionic dyes tend to aggregate in solution which is related to dye concentration.[28] It was reported in literature that MB exists in a single molecular state in aqueous solution up to 30 mg L^{-1}, while at a concentration > 60 mg L^{-1} it tends to form aggregates.[29] This probably is the reason behind the similar retention efficiency of M52, E52 and P52 for 100 mg L^{-1} feed solution.

From Figure 2 it is evident that M52 and P52 have relatively obvious differences in hydrophilicity. Therefore, we compared the pure water flux (**Figure 4a**) and MB rejection from 10 mg L^{-1} aqueous solution (Figure 4b) of membranes with a series of different degrees of quaternization with MeI and 1-PrI, namely M12, M25, M42, M52, M100, P12, P25, P42, P52 and P55 (the letters M and P stand for MeI and 1-PrI while the following number stands for the degree of quaternization, respectively). A decrease of the pure water flux and an increase of MB rejection were observed with the increase of the degree of quaternization. These results demonstrate that the effective pore size of both of the series of quaternized membranes was successfully tailored by controlling the degree of quaternization in a wide range. For the same degree of conversion (in the range 12 – 52%), the membranes quaternized by 1-PrI had higher water flux and lower MB retention compared to MeI, which proves again that the effective pore size can be tuned by controlling the size of alkyl groups. A sharp increase of MB retention was observed for M25 compared to M12. A similar increase of MB retention was also observed for

P42 compared to P25. Moreover, it is noteworthy that the MB retention of M25 was dramatically increased compared to P25. These results suggest that the effective pore size of the membranes must cross a minimum limit for high retention of MB. Hence, Figure 4b reconfirms that the retention of MB was largely caused by the size exclusion. Efforts have been made to predict the pore size at the surface of the SNIPS membrane from the ration of pure water flux using a relationship derived from Hagen- Poiseuille equation.[18, 20] However, there are several limitations to obtain the absolute pore size from the ratio of pure water flux (detailed discussion is in the Supporting Information, section 2.3.4). At this stage it is not possible for us to predict the absolute effective pore size of the quaternized membranes in the hydrated state. According to MM2 force field calculation (by chem3D software package), the molecular size of MB is 1.1 nm which is consistent with the values reported in literature.[30] As we have successfully tuned the retention of MB between 6 – 98% (Figure 4b), in spite of the limitation to determine the absolute value of the pore size in the hydrated state, it is clear that the pore size of the PS-*b*-P4VP membrane can be successfully tuned in the nanofiltration regime by quaternization of pore-forming P4VP blocks.

The membrane fabrication and post-modification method presented in this work is promising for the production of next generation nanofiltration membranes. The PS-*b*-P4VP membrane prepared by SNIPS had an isoporous layer of well-defined cylindrical channels. By using a scalable heterogeneous gas-solid reaction the homogeneity of the quaternization was successfully controlled. The effective pore size of the membrane in the hydrated state was successfully tuned in a wide range by changing the size of the alkyl groups of the quaternization agent and the degree of quaternization. The excellent performance of the membrane to separate the cationic MB from aqueous solution demonstrated the potential of these membranes for nanofiltration applications. Future research should be directed towards improving the

fundamental understanding of transport and rejection behavior of these membranes for water purification, wastewater treatment, biomolecule separation etc.

Supporting Information

Supporting Information is available from the Wiley Online Library or from the author.

Acknowledgements: The authors thank Anke-Lisa Metze, Silvio Neumann, Maren Brinkmann for characterizations of the block copolymer and membranes, Brigitte Lademann for technical support of synthesis of the block copolymer, Thomas Bucher and Christian Höhme for helpful discussions.

Received: Month XX, XXXX; Revised: Month XX, XXXX; Published online:

Keywords: block copolymers, isoporous membranes, membrane postmodification, water purification, polyelectrolytes

[1] a) R. van Reis, A. Zydney, *J. Membr. Sci.* **2007**, *297*, 16; b) Y. Yang Seung, J. Park, J. Yoon, M. Ree, K. Jang Sung, K. Kim Jin, *Adv. Funct. Mater.* **2008**, *18*, 1371; c) M. A. Shannon, P. W. Bohn, M. Elimelech, J. G. Georgiadis, B. J. Marinas, A. M. Mayes, *Nature* **2008**, *452*, 301; d) X. Peng, J. Jin, Y. Nakamura, T. Ohno, I. Ichinose, *Nat. Nanotechnol.* **2009**, *4*, 353; e) G. Han, T.-S. Chung, M. Weber, C. Maletzko, *Environ. Sci. Technol.* **2018**, *52*, 3676; f) G. Han, Y. Feng, T. S. Chung, M. Weber, C. Maletzko, *Environ. Sci. Technol.* **2017**, *51*, 14254; g) X. Feng, M. E. Tousley, M. G. Cowan, B. R. Wiesenauer, S. Nejati, Y. Choo, R. D. Noble, M. Elimelech, D. L. Gin, C. O. Osuji, *ACS Nano* **2014**, *8*, 11977; h) X. Feng, S. Nejati, M. G. Cowan, M. E. Tousley, B. R. Wiesenauer, R. D. Noble, M. Elimelech, D. L. Gin, C. O. Osuji, *ACS Nano* **2016**, *10*, 150.

[2] F. S. Bates, M. A. Hillmyer, T. P. Lodge, C. M. Bates, K. T. Delaney, G. H. Fredrickson, *Science* **2012**, *336*, 434.

[3] K. V. Peinemann, V. Abetz, P. F. Simon, *Nat. Mater.* **2007**, *6*, 992.

[4] V. Abetz, *Macromol. Rapid Commun.* **2015**, *36*, 10.

[5] a) A. Jung, S. Rangou, C. Abetz, V. Filiz, V. Abetz, *Macromol. Mater. Eng.* **2012**, *297*, 790; b) J. Hahn, V. Filiz, S. Rangou, J. Clodt, A. Jung, K. Buhr, C. Abetz, V. Abetz, *J. Polym. Sci., Part B: Polym. Phys.* **2013**, *51*, 281; c) J. Hahn, V. Filiz, S. Rangou, B. Lademann, K. Buhr, J. I. Clodt, A. Jung, C. Abetz, V. Abetz, *Macromol. Mater. Eng.* **2013**, *298*, 1315; d) A. Jung, V. Filiz, S. Rangou, K. Buhr, P. Merten, J. Hahn, J. Clodt, C. Abetz, V. Abetz, *Macromol. Rapid Commun.* **2013**, *34*, 610; e) S. Saleem, S. Rangou, C. Abetz, B. Lademann, V. Filiz, V. Abetz, *Polymers* **2017**, *9*, 216; f) W. A. Phillip, R. M. Dorin, J. Werner, E. M. Hoek, U. Wiesner, M. Elimelech, *Nano Lett.* **2011**, *11*, 2892; g) R. A. Mulvenna, J. L. Weidman, B. Jing, J. A. Pople, Y. Zhu, B. W. Boudouris, W. A. Phillip, *J. Membr. Sci.* **2014**, *470*, 246; h) C. Höhme, J. Hahn, B. Lademann, A. Meyer, B. Bajer, C. Abetz, V. Filiz, V. Abetz, *Eur. Polym. J.* **2016**, *85*, 72; i) J. I. Clodt, S. Rangou, A. Schröder, K. Buhr, J. Hahn, A. Jung, V. Filiz, V. Abetz, *Macromol. Rapid Commun.* **2013**, *34*, 190.

[6] a) T. Bucher, V. Filiz, C. Abetz, V. Abetz, *Membranes (Basel)* **2018**, *8*; b) J. Hahn, J. I. Clodt, C. Abetz, V. Filiz, V. Abetz, *ACS Appl. Mater. Interfaces* **2015**, *7*, 21130.

[7] a) K. Sankhala, J. Koll, V. Abetz, *ACS Macro Lett.* **2018**, *7*, 840; b) N. Noor, J. Koll, M. Radjabian, C. Abetz, V. Abetz, *Macromol. Rapid Commun.* **2016**, *37*, 414.

[8] a) M. Radjabian, C. Abetz, B. Fischer, A. Meyer, V. Abetz, *ACS Appl. Mater. Interfaces* **2017**, *9*, 31224; b) W. A. Phillip, M. A. Hillmyer, E. L. Cussler, *Macromolecules* **2010**, *43*, 7763; c) S. Dami, C. Abetz, B. Fischer, M. Radjabian, P. Georgopanos, V. Abetz, *Polymer* **2017**, *126*, 376.

[9] a) R. M. Dorin, W. A. Phillip, H. Sai, J. Werner, M. Elimelech, U. Wiesner, *Polymer* **2014**, *55*, 347; b) S. Rangou, K. Buhr, V. Filiz, J. I. Clodt, B. Lademann, J. Hahn, A. Jung, V. Abetz, *J. Membr. Sci.* **2014**, *451*, 266.

[10] M. Radjabian, V. Abetz, *Adv. Mater.* **2015**, *27*, 352.

[11] H. Yu, X. Qiu, S. P. Nunes, K. V. Peinemann, *Angew. Chem., Int. Ed.* **2014**, *53*, 10072.

[12] a) S. D. Tillmann, I. Cekic‐Laskovic, M. Winter, K. Loos, *Energy Technol.* **2017**, *5*, 715; b) Y. Gu, J. G. Werner, R. M. Dorin, S. W. Robbins, U. Wiesner, *Nanoscale* **2015**, *7*, 5826; c) I. Vukovic, S. Punzhin, V. S. D. Voet, Z. Vukovic, J. T. M. de Hosson, G. ten Brinke, K. Loos, *J. Vis. Exp.* **2014**, 50673; d) G. G. du Sart, I. Vukovic, Z. Vukovic, E. Polushkin, P. Hiekkataipale, J. Ruokolainen, K. Loos, G. ten Brinke, *Macromol. Rapid Commun.* **2011**, *32*, 366; e) I. Vukovic, S. Punzhin, Z. Vukovic, P. Onck, J. T. M. De Hosson, G. ten Brinke, K. Loos, *ACS Nano* **2011**, *5*, 6339.

[13] a) T. Segal-Peretz, J. Winterstein, M. Doxastakis, A. Ramírez-Hernández, M. Biswas, J. Ren, H. S. Suh, S. B. Darling, J. A. Liddle, J. W. Elam, *ACS Nano* **2015**, *9*, 5333; b) T. Segal-Peretz, C. Zhou, J. Ren, T. Dazai, L. E. Ocola, R. N. S. Divan, P. F. Nealey, *J. Photopolym. Sci. Technol.* **2016**, *29*, 653; c) C. Zhou, T. Segal-Peretz, M. E. Oruc, H. S. Suh, G. Wu, P. F. Nealey, *Adv. Funct. Mater.* **2017**, *27*, 1701756.

[14] J. I. Clodt, V. Filiz, S. Rangou, K. Buhr, C. Abetz, D. Höche, J. Hahn, A. Jung, V. Abetz, *Adv. Funct. Mater.* **2013**, *23*, 731.

[15] D. Keskin, J. I. Clodt, J. Hahn, V. Abetz, V. Filiz, *Langmuir* **2014**, *30*, 8907.

[16] J. Wang, M. M. Rahman, C. Abetz, S. Rangou, Z. Zhang, V. Abetz, *Macromol. Rapid Commun.* **2018**, e1800435.

[17] a) S. P. Nunes, M. Karunakaran, N. Pradeep, A. R. Behzad, B. Hooghan, R. Sougrat, H. He, K.-V. Peinemann, *Langmuir* **2011**, *27*, 10184; b) Q. Zhang, Y. Gu, Y. M. Li, P. A. Beaucage, T. Kao, U. Wiesner, *Chem. Mater.* **2016**, *28*, 3870.

[18] Y. Gu, U. Wiesner, *Macromolecules* **2015**, *48*, 6153.

[19] Y. Zhang, R. A. Mulvenna, S. Qu, B. W. Boudouris, W. A. Phillip, *ACS Macro Lett.* **2017**, *6*, 726.

[20] Y. Su, Y. Liu, T. Liu, X. Wang, *J. Appl. Polym. Sci.* **2018**, 47137.

[21] B. P. Tripathi, N. C. Dubey, S. Choudhury, F. Simon, M. Stamm, *J. Mater. Chem. B* **2013**, *1*, 3397.

[22] X. Qiu, H. Yu, M. Karunakaran, N. Pradeep, S. P. Nunes, K.-V. Peinemann, *ACS Nano* **2013**, *7*, 768.

[23] Y. Miyaki, H. Nagamatsu, M. Iwata, K. Ohkoshi, K. Se, T. Fujimoto, *Macromolecules* **1984**, *17*, 2231.

[24] H. Lee, K. Char, *ACS Appl. Mater. Interfaces* **2009**, *1*, 913.

[25] D. M. Stachera, R. F. Childs, *J. Membr. Sci.* **2001**, *187*, 213.

[26] M. H. Park, C. Subramani, S. Rana, V. M. Rotello, *Adv. Mater.* **2012**, *24*, 5862.

[27] X.-L. Wang, T. Tsuru, S.-i. Nakao, S. Kimura, *J. Membr. Sci.* **1997**, *135*, 19.

[28] L. Antonov, G. Gergov, V. Petrov, M. Kubista, J. Nygren, *Talanta* **1999**, *49*, 99.

[29] a) K. Fujita, K. Taniguchi, H. Ohno, *Talanta* **2005**, *65*, 1066; b) T. Hinoue, Y. Yokoyama, T. Ozeki, *Jpn Analyst* **1994**, *43*, 443.

[30] a) X. Feng, K. Kawabata, G. Kaufman, M. Elimelech, C. O. Osuji, *ACS Nano* **2017**, *11*, 3911; b) J. d. S. Macedo, N. B. da Costa Júnior, L. E. Almeida, E. F. d. S. Vieira, A. R. Cestari, I. d. F. Gimenez, N. L. Villarreal Carreño, L. S. Barreto, *J. Colloid Interface Sci.* **2006**, *298*, 515.

Figure 1. (a) Reaction scheme of quaternization of the PS-*b*-P4VP membrane. (b) ATR-FTIR spectra of I0 and M100. (c) ^{1}H NMR spectra of I0 and M100. Secondary electron (SE) images of SEM: cross section and top surface (d, e) I0, (g, h) M100. Back scattered electron (BSE) images of SEM: top surface of (f) I0, (i) M100.

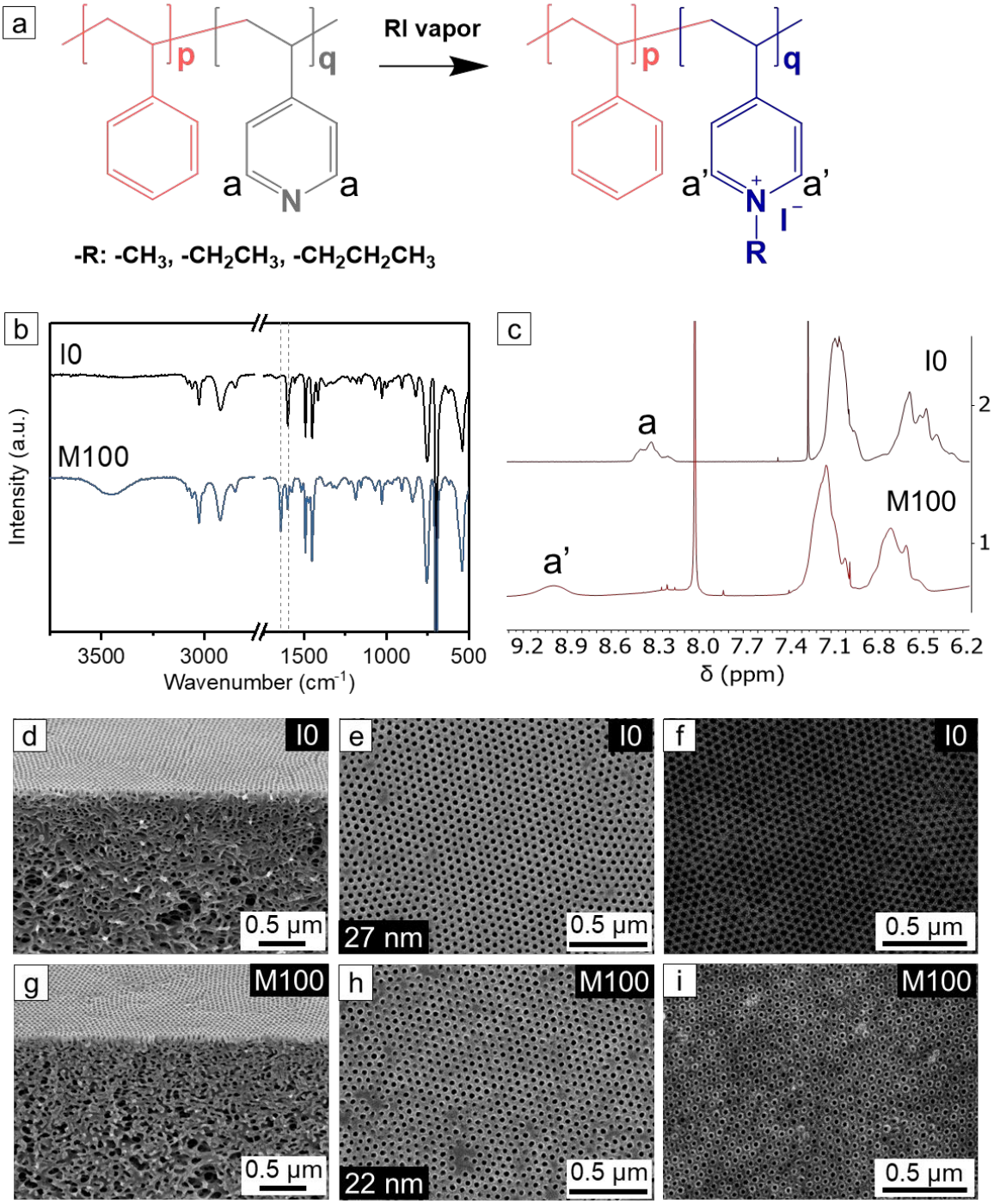

Figure 2. (a) Snapshots of dynamic contact angle of a water droplet onto I0 surface. (b) The change of contact angles onto I0, M52, E52 and P52 surface with time. (c) Water flux of I0, M52, E52 and P52 at a transmembrane pressure up to 1 bar at room temperature. Secondary electron (SE) images of SEM: top surface of (d) M52, (e) E52, (f) P52. (g) Schematic representation of I0, M52, E52 and P52 in the hydrated state.

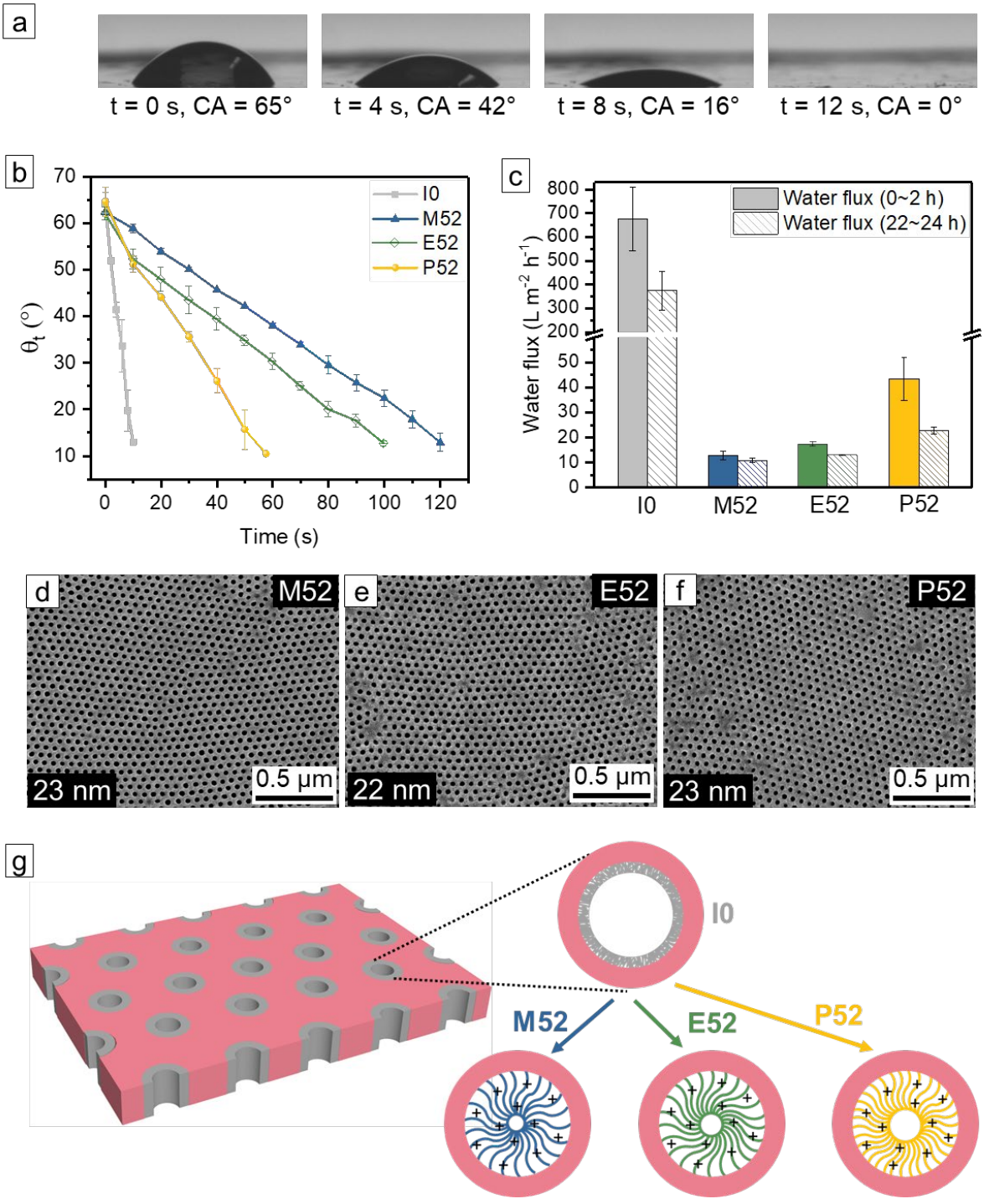

Figure 3. (a) Molecular structure and space-filling model of methylene blue (MB). (b) The photography of the feed and permeate solutions of I0, M52, E52, and P52, and the prepared membranes after MB rejection measurements using a 10 mg L^{-1} feed solution. (c) UV-vis absorbance of the feed and the permeate solutions of I0, M52, E52, and P52 with feed solution of concentration 10 mg L^{-1}. (d) MB retention of I0, M52, E52, and P52 with feed solution of concentration 10 mg L^{-1}.

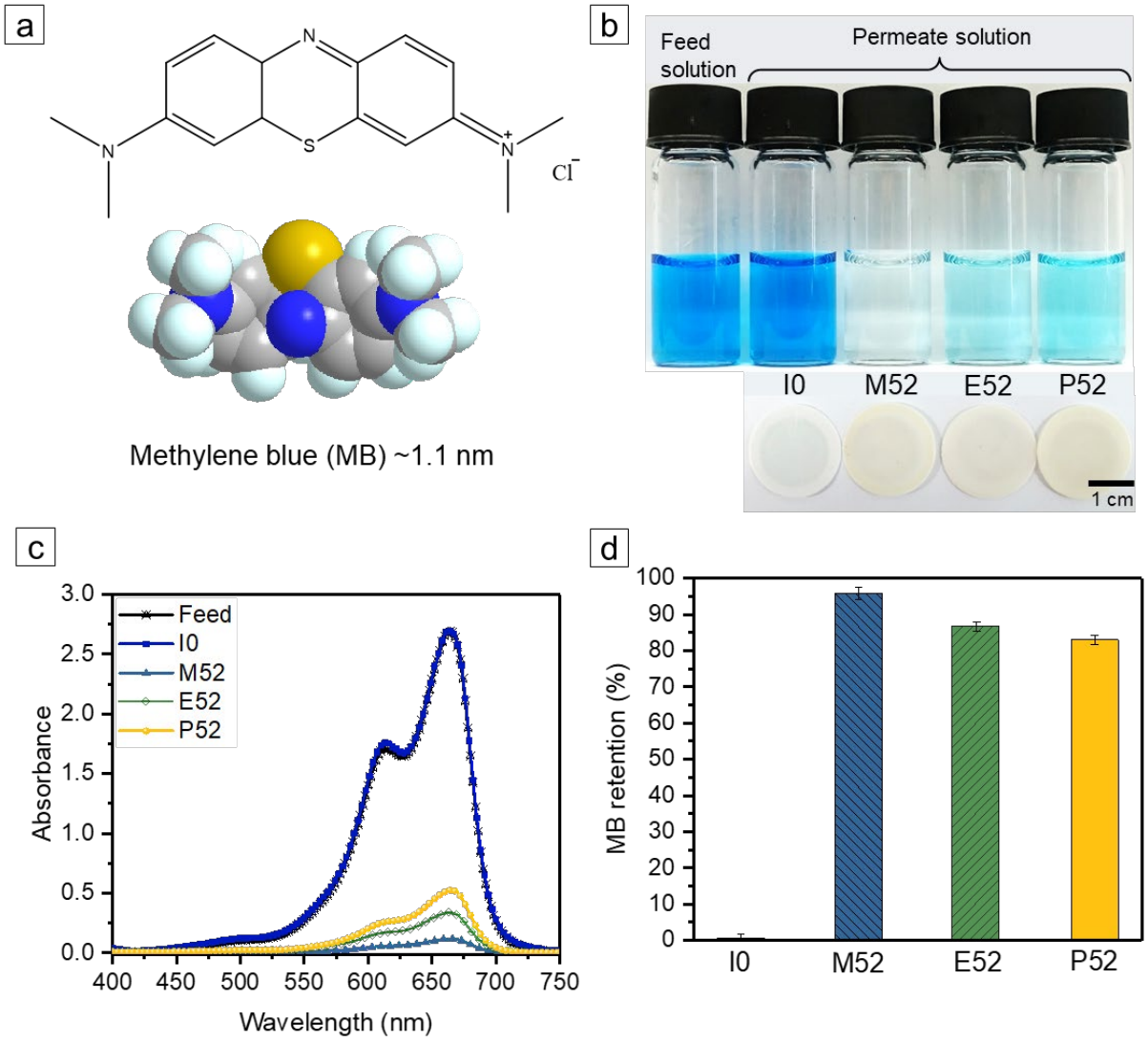

Figure 4. (a) Water flux (average value of 0~2 h measurement) of I0 and the membranes having the series of different degrees of quaternization with MeI and 1-PrI, respectively. (b) MB retention of I0 and the membranes having the series of different degrees of quaternization with MeI and 1-PrI, respectively, with feed solution of concentration 10 mg L^{-1}.